

**Hierarchical population model with a carrying capacity distribution for bacterial biofilms**J. O. Indekeu<sup>1</sup> and K. Sznajd-Weron<sup>2</sup><sup>1</sup>*Laboratory for Solid-State Physics and Magnetism, Katholieke Universiteit Leuven, Leuven, Belgium*<sup>2</sup>*Institute for Theoretical Physics, University of Wrocław, Wrocław, Poland*

(Received 19 December 2002; revised manuscript received 23 July 2003; published 17 December 2003)

In order to describe biological colonies with a conspicuous hierarchical structure, a time- and space-discrete model for the growth of a rapidly saturating local biological population  $N(x,t)$  is derived from a hierarchical random deposition process previously studied in statistical physics. Two biologically relevant parameters, the probabilities of birth,  $B$ , and of death,  $D$ , determine the carrying capacity  $K$ . Due to the randomness the population depends strongly on position  $x$  and there is a distribution of carrying capacities,  $\Pi(K)$ . This distribution has self-similar character owing to the exponential slowing down of the growth, assumed in this hierarchical model. The most probable carrying capacity and its probability are studied as a function of  $B$  and  $D$ . The effective growth rate decreases with time, roughly as in a Verhulst process. The model is possibly applicable, for example, to bacteria forming a “towering pillar” biofilm, a structure poorly described by standard Eden or diffusion-limited-aggregation models. The bacteria divide on randomly distributed nutrient-rich regions and are exposed to a random local bactericidal agent (antibiotic spray). A gradual overall temperature or chemical change away from optimal growth conditions reduces bacterial reproduction, while biofilm development degrades antimicrobial susceptibility, causing stagnation into a stationary state.

DOI: 10.1103/PhysRevE.68.061904

PACS number(s): 87.68.+z, 47.53.+n

**I. INTRODUCTION: RELEVANCE OF FRACTAL GEOMETRY TO BACTERIAL COLONIES**

In opening this paper it is useful to review concisely the relevance of fractal geometry to the morphology of bacterial colonies. We distinguish two cases. If nutrient supply is not limited, compact colonies grow according to a simplified spontaneous multiplication process proposed by Eden in 1961 [1]. In spite of its compactness, an Eden cluster displays a rough surface with self-affine fractal geometry. In 1990 experimental evidence was presented for this kind of anisotropic fractal scaling of the shape of a biological system, in the surface of colonies of *Escherichia coli* and *Bacillus subtilis* growing on agar plates [2]. On the other hand, if the growth is limited by nutrient diffusion, it was first observed in 1989 that the entire colonies—not just their surfaces—develop a self-similar fractal shape [3]. This pattern corresponds to the geometry of diffusion limited aggregation (DLA) [4] and has been seen in many experiments to date on bacterial colonies on low-nutrient substrates, in the form of branching growth with or without chirality [5].

For biofilms specifically, fractal structure was uncovered with the aid of confocal laser scanning microscopy (CLSM) and a (volume) fractal dimension was determined for biomass clusters of sizes exceeding 5  $\mu\text{m}$  up to several hundred microns [14], while smaller aggregates are compact. A two-dimensional cellular automata approach taking into account cell division, nutrient diffusion and convection, and cell detachment was applied to simulate dynamically a wide range of biofilm morphologies, including mushroom- and tower- or tuliplike structures [15]. Clearly, neither Eden nor DLA modeling is adequate for describing these forms. In view of the conspicuous hierarchical structure of several of these morphologies, revealed by CLSM, the simple model proposed in this paper may provide a basic alternative in arbitrary space dimension.

**II. THE MODEL**

As a concrete example, consider bacteria on a line with local population  $N(x,t)$  defined on  $x \in [0,1]$ . The population is normalized, so that  $N$  is to be interpreted as a density rather than the number of bacteria. Generalization to two or three space dimensions is straightforward, as will become clear from the simple structure of the model. Assume, for simplicity, a homogeneous initial condition  $N_0 = N(x,0) > 0$ , representing inoculation along the line of a thin uniform layer. At  $t > 0$  the growth process is characterized by a probability of birth,  $B$ , which is applied to segments or “patches” along the line. The stochastic character of the growth reflects that the surface is inhomogeneous. Some areas are nutrient rich (e.g., agar), others are not. The division process is effective only in nutrient-rich patches. These patches are assumed to be of characteristic size  $1/\lambda$ , where  $\lambda$  is a scale factor central to the model. Alternative ways of inducing spatially nonuniform growth or depletion are to apply, for photosynthetic bacteria, favorable or unfavorable (UV) illumination according to a structured or random spatial pattern [6,7].

Besides nutrient nonuniformity, the environmental conditions are locally modified in a random way, for example, by spraying drops of an antibiotic which subsequently spreads by diffusion or transport resulting from bacterial motility. In places with low chemical concentration the population stagnates, elsewhere it shrinks. The action of the bactericidal product is expressed through a probability of death,  $D$ . An interesting variant on antibiotics, and relevant in particular to inhibition of biofilm formation, is a nutrient remover such as, for example, lactoferrin. This protein, which is abundant in human external secretions, mops up traces of iron and thereby deprives bacteria of an essential substance. Applied in concentrations below those that kill or prevent growth, it just slightly increases the division time of the bacteria and enhances their surface motility, causing them to “twitch” or

wander around seeking food. As a result, microcolonies do not form and matrix-encased communities specialized for surface persistence (biofilms) do not develop [8].

The model is composed as follows. The characteristic size of the spatial inhomogeneity of the nutrient is, for simplicity, taken to be the same as that of the applied antimicrobial perturbation. The (unit) line is thus divided in  $\lambda$  segments, each of which has the size of, say, an antibiotic drop. The probability of birth,  $B$ , is applied to each segment, and subsequently the probability of death,  $D$ . Each segment is thus visited twice. We have  $0 \leq B, D \leq 1$ , and without loss of generality we take  $\lambda=3$  in this paper.

One generation later this process is repeated, but the maximum local increase or decrease of the population is reduced by a factor of  $\lambda$ . This reduction is repeated in every generation. In this way the growth process eventually comes to a halt, and the population approaches a *carrying capacity*, as is commonly the case in models for a single species [9]. This rescaling of the growth or the depletion is a crucial ingredient of the model and leads to a hierarchical buildup of the population. While introduced here heuristically, various biologically relevant experimental conditions can be thought of, for which this rescaling is an adequate simple approximation for modeling a gradual saturation of the population. Indeed, bacterial reproductivity and/or susceptibility to antimicrobial agents can “wear out” in a systematic manner, uniformly in space. For example, the *effective birth rate* decreases significantly by varying the temperature some 10 °C away from optimal growth conditions. Also, once a biofilm starts forming, it becomes resistant to nutrient removers such as lactoferrin, and it notoriously resists killing by antibiotics. Further, if there is no nutrient-supplying fluid surrounding the bacterial colony, or if it stops flowing, convective mass transport is not available and much slower diffusive transport sets in without nutrient renewal. The precise way in which this saturation is imposed here, through a constant rescaling factor, has been deliberately chosen so as to reproduce the exponential convergence characteristic of a standard Verhulst process, in the continuum-time approximation of our model (see Sec. III).

Further, the rescaling by a factor of  $\lambda$  is applied not only to the increase or decrease of the local population, but also to the typical size of the nutrient-rich or bactericidal patches. This assumption can be justified as follows. Since after one generation (of the order of 2 h in real time) the nutrient or chemical contamination has been redistributed in space, mainly by diffusion or by bacterial motion, regions which were initially rich (or pure) will show poor (or toxic) spots, while initially barren regions will display small fertile areas. We restrict attention to the case of negligible convective transport through the surrounding fluid, since convection would clearly invalidate our assumption of decreasing redistribution of mass in smaller and smaller fragments in the course of time. Thus, we apply the random birth and death rules on an ever smaller length scale, reduced by a factor of  $\lambda$  with respect to the previous generation, and repeat this reduction generation after generation.

In sum, in every new generation the population fluctuations are reduced by cooling (or heating), or by lack of nu-

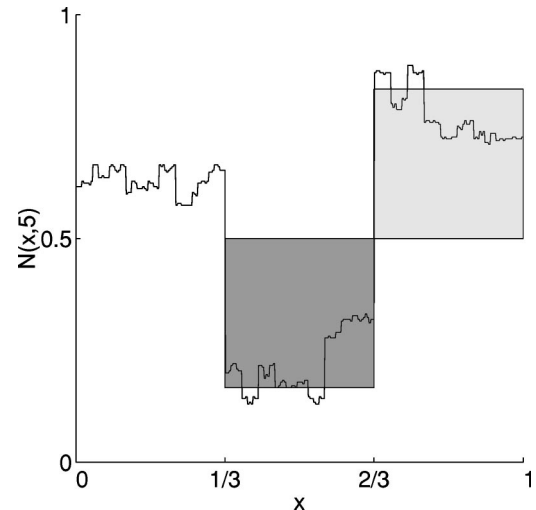


FIG. 1. Sample of a local population density after five generations of hierarchical random growth with  $B=0.5$  and  $D=0.2$ ,  $N(x,5)$ . The rescaling factor is  $\lambda=3$ . The initial population is  $N(x,0)=0.5$ . The light (dark) gray area indicates the massive growth (depletion) which occurred in the first generation. As a result, large jumps at  $x=1/3$  and  $x=2/3$  persist for all later times.

trient flow, and by biofilm development, and they occur on a smaller length scale due to diffusive nutrient/antibiotic fragmentation. A single scale factor controls—in this greatly simplified model—all these dynamical complications, so that neither external time-dependent fields nor “interparticle” interactions occur explicitly in what follows. Repeating this process saturation is reached exponentially rapidly, typically in less than ten generations, as the calculations show. The resulting local population density for long times,  $N(x,\infty)$ , is highly inhomogeneous and largely reflects the initial random distribution of the nutrient distribution and the toxic contamination, brought about by spraying. Considered mathematically,  $N(x,\infty)$  is a fractal curve with infinite length, but trivial fractal dimension  $d_F=1$ . Figure 1 shows an example of  $N(x,5)$ , the local population after five generations, assuming  $B=0.5$  and  $D=0.2$ .

Note that the natural death of the organisms is not included explicitly in the model, for the simple reason that the induced saturation occurs on a time scale (several hours) significantly shorter than the natural lifetime. In other words, the probability  $D$  pertains to death caused by bactericidal products alone.

In Fig. 1 it can be seen that what happens in the first generation dominates the future evolution. For example, the light gray square represents the massive growth on a nutrient-rich segment  $(2/3,1)$  while the dark gray square indicates the result of the killing of most of the bacteria on a toxic patch  $(1/3,2/3)$ . In the first segment  $(0,1/3)$  nothing happened in the first generation. After a few generations the population “landscape” consists of towers and deep crests, which get rougher as time progresses, but which hardly change size anymore.

This model is mathematically equivalent to the previously introduced hierarchical random deposition process [10] with rescaling factor  $\lambda$ , and probabilities  $P=B(1-D)$  for depos-

iting a hill, and  $Q=D(1-B)$  for digging a hole, with  $P+Q \leq 1$ . The correspondence between  $(B,D)$  and  $(P,Q)$  can be seen by taking into account that in the biological application every segment is visited twice, applying  $B$  in the first visit followed by  $D$  in the second, whereas in the deposition model there is only one visit per segment, per generation. Therefore, after a complete visit the population is increased, provided offspring was produced *and* no deaths occurred, whence the product  $B(1-D)$ . The population is decreased provided no divisions occurred *and* the antibiotics killed a fraction of the existing population, whence  $(1-B)D$ . Finally, the population remains constant if *either* offspring was produced but subsequently killed, *or* no births took place and the antibiotics were absent or had no effect. The probability for this is  $BD+(1-B)(1-D)=1-(P+Q)$ . Note that the total probability for the three outcomes is unity.

Using the deposition model it is easy to derive analytical results in terms of the variables  $P$  and  $Q$ , and also numerical simulation is straightforward. In generation  $n$  the process requires just  $\lambda^n$  (pseudo-)random numbers. For each segment of width  $\lambda^{-n}$  along  $x$  the population is increased by an amount equal to the segment size (in dimensionless units) with probability  $P$ , or reduced by that amount with probability  $Q$ , or left unchanged with probability  $1-(P+Q)$ . This leads to the characteristic rapidly converging population landscape formed by squares of decreasing size (Fig. 1).

The initial condition is taken to be  $N_0=1/(\lambda-1)$ , independent of  $x$  (uniform inoculation). The first quantity of interest is the mean carrying capacity  $\bar{K}$ , which is the ensemble average of  $N(x,\infty)$  over all possible random realizations of the process. Since on average the population grows by an amount  $(B-D)\lambda^{-n}$  in generation  $n$ , we obtain

$$\bar{K}=(1+B-D)/(\lambda-1)=(1+P-Q)/(\lambda-1), \quad (2.1)$$

independent of  $x$ . Clearly, the initial condition  $N_0$  has been chosen large enough so that, for all  $B$  and  $D$ , the population remains positive for all  $x$  and  $t$ , and approaches zero only in the extinction limit  $B=0, D=1$ . Note the simple identity  $B-D=P-Q$ , making the relations between the growth probabilities and the deposition parameters more transparent.

Generalization of the model to higher dimensions (e.g., substrate dimension 2) is not pursued here, but the results of such extension can easily be anticipated by examining the landscapes shown for the hierarchical deposition model [10,11] on planar substrates. In fact, if the bacterial population is compact, the value of  $N(x,t)$  is simply proportional to the height of the biofilm above the substrate, and the landscapes can be interpreted as three-dimensional in real space. This correspondence holds as long as there are no ‘‘overhangs’’ or holes in the biofilm, and thus works for compact towering pillar structures but not for noncompact or mushroom-shaped ones [8]. The similarity between the three-dimensional characteristic landscapes generated in this model, and the structure of its horizontal cross section [11] (see Fig. 6 in that reference), and images of vertical and horizontal sections of a towering pillar biofilm, as obtained by confocal laser scanning microscopy, is remarkable [12]. This suggests that a hierarchical model may be a reasonable

first approximation for describing this type of biofilm growth. Towerlike structures do not emerge in the Eden model or DLA models, which are the established paradigms of fractal bacterial colony models.

The connection between the model and the familiar Verhulst process is elucidated in Sec. III. It is made clear that  $B$  and  $D$  are biologically relevant parameters determining the carrying capacity  $K$ , whereas the role of  $\lambda$  is to induce exponentially rapid saturation, ubiquitously found when a biological population approaches the carrying capacity of its environment. Further,  $\lambda$  also sets an overall time scale factor. The carrying capacity distribution, the key result of this random growth model, is calculated analytically in Sec. IV, and concrete examples are discussed in Sec. V, together with a check against numerical simulation. The self-similar character of this  $K$  distribution is demonstrated and the effect of  $B$  and  $D$  on the standard deviation of the population is examined in representative cases. Section VI deals with the most probable carrying capacity and its probability, considered as a function of  $B$  and  $D$ . Insight is gained in the abundance of large deviations away from the most probable  $K$ . Section VII presents our conclusions and addresses a possible experimental test of this model.

### III. CONNECTION WITH A VERHULST PROCESS OR LOGISTIC GROWTH

In this section we are concerned with the uniform, i.e., spatially averaged, population. The time evolution of the mean, or ‘‘quenched average,’’ of  $N(x,t)$  is given by the change in the mean value,  $\bar{N}(t)$ , from  $t=n$  to  $t=n+1$ ,

$$\bar{N}(n+1)=\bar{N}(n)+\lambda^{-n-1}(B-D), \quad (3.1)$$

which is solved by

$$\bar{N}(n)=N_0+(1-\lambda^{-n})(B-D)/(\lambda-1). \quad (3.2)$$

This is a simple growth, converging exponentially rapidly, for  $n \rightarrow \infty$ , to the mean carrying capacity. Clearly, the role of the rescaling factor  $\lambda$  in the model is to generate this simple saturation. It is useful now to work with the differences

$$\Delta\bar{N}=\bar{N}-N_0 \quad \text{and} \quad \Delta\bar{K}=\bar{K}-N_0, \quad (3.3)$$

with respect to the initial population  $N_0=1/(\lambda-1)$ . We obtain

$$\Delta\bar{N}(n)=(1-\lambda^{-n})\Delta\bar{K}. \quad (3.4)$$

Using this in Eq. (3.1) leads to

$$\Delta\bar{N}(n+1)-\Delta\bar{N}(n)=\frac{\lambda-1}{\lambda} \frac{\lambda^{-n}}{1-\lambda^{-n}} \Delta\bar{N}(n). \quad (3.5)$$

For large  $n$ , we can neglect  $\lambda^{-n}$  compared to 1 in the denominator, and again using Eq. (3.4), we get the *nonlinear* difference equation

$$\Delta\bar{N}(n+1) - \Delta\bar{N}(n) \approx \frac{\lambda-1}{\lambda} \Delta\bar{N}(n) \left( 1 - \frac{\Delta\bar{N}(n)}{\Delta\bar{K}} \right). \quad (3.6)$$

This is clearly a discrete Verhulst process, the continuum time limit of which is of the form of the Verhulst equation

$$\frac{d\Delta\bar{N}(t)}{dt} = \frac{\lambda-1}{\lambda} \Delta\bar{N}(t) \left( 1 - \frac{\Delta\bar{N}(t)}{\Delta\bar{K}} \right). \quad (3.7)$$

Note that, in general, the discrete time model and its continuum time limit have slightly different asymptotic behavior for long times, but this is irrelevant for our discussion here.

This analogy allows us to identify and interpret the model parameters unambiguously. The characteristic “bare decay rate” or saturation time scale of the model is  $\lambda/(\lambda-1)$ , a constant. The precise value of the length rescaling factor  $\lambda$  in the model has no particular biological relevance, apart from affecting slightly the morphology of the population landscape, and can be chosen to be an arbitrary integer  $\lambda > 1$ . The carrying capacity (difference) given by  $\Delta\bar{K} = (B-D)/(\lambda-1)$  is an important property, and we find that it is determined simply by the difference of the birth and death rates. This link between a phenomenological parameter of the Verhulst equation, the carrying capacity, and the stochastic “microscopic” model parameters  $B$  and  $D$  is a key ingredient of our model. Finally, the *effective* birth rate  $1/\tau$ , which is by definition the ratio  $[d\Delta\bar{N}(t)/dt]/\Delta\bar{N}(t)$ , depends on the size of the population, and eventually vanishes as the carrying capacity is approached, as is typical of logistic growth. Asymptotically for long times, it is given by

$$1/\tau \sim \frac{\lambda-1}{\lambda} \left( 1 - \frac{\Delta\bar{N}(t)}{\Delta\bar{K}} \right) = \frac{\lambda-1}{\lambda} \lambda^{-n}. \quad (3.8)$$

More precisely, the exact expression for all times, as follows from Eq. (3.5), is

$$1/\tau = \frac{\lambda-1}{\lambda} \frac{\lambda^{-n}}{1-\lambda^{-n}}. \quad (3.9)$$

Note, and we wish to stress, that for our process the Verhulst equation is nothing but an easily interpretable *nonlinear* approximation to the actual linear differential equation describing our dynamics,

$$\begin{aligned} \frac{d\Delta\bar{N}(t)}{dt} &= \frac{\lambda-1}{\lambda} \Delta\bar{N}(t) \left( 1 - \frac{\Delta\bar{N}(t)}{\Delta\bar{K}} \right) \frac{\Delta\bar{K}}{\Delta\bar{N}(t)} \\ &= \frac{\lambda-1}{\lambda} [\Delta\bar{K} - \Delta\bar{N}(t)]. \end{aligned} \quad (3.10)$$

The precise way (in our case exponential) in which the effective birth rate vanishes is only one possible way in which this rate in a biological system can be driven away from its optimal value. We envisage that this drift is achieved by cutting the nutrient supply, or by a temperature variation,

upwards or downwards, bringing the bacterial growth to a halt on a time scale of a small number of generations. In Sec. II we already alluded to the fact that biofilm development can be a factor leading to resistance to antibiotics, which can lead to a vanishing death rate. We simply assume that both effects (e.g., nutrient embargo and biofilm formation) occur uniformly throughout the sample. Our justification for assuming a uniform external perturbation responsible for the saturation is that in our random model the effective birth rate (3.9) does not depend on the local ( $x$ -dependent) population, but only on time. Alternatively, the self-limitation of the population could of course also be due to *local* overpopulation, but this model is in its present form too simple to allow for an internal local feedback process.

#### IV. THE CARRYING CAPACITY DISTRIBUTION

Even though the average growth of the population is characterized by simple exponential saturation, the local population  $N(x,t)$  for a particular realization of the quenched randomness typically shows interesting large fluctuations. These deviations, highly nonuniform in space, can possibly be measured experimentally by probing the local population of bacteria after spraying a few drops of an antibiotic. The fluctuations of the total population  $\mathcal{N}(t) = \int_0^1 N(x,t) dx$  are studied in this section and the following two.

Our aim in this section is to explore the effect of random nutrient inhomogeneity and random antibiotic spray on the carrying capacity  $K$ , which is the asymptotic value for long times of the total population. The simple stochastic nature of the model allows to obtain the full  $K$  distribution in analytic form in terms of the probability of birth  $B$  and that of death  $D$ , with modest mathematical effort. Consider a particular random evolution. In generation  $m$  the total population grows by an amount  $(\lambda^m - k_m)/\lambda^{2m}$  where the possible values of the integer  $k_m$  are contained in the set  $\{0, 1, \dots, 2\lambda^m\}$ . For example, in the deterministic limits  $B=1$  and  $D=0$ , one always has  $k_m=0$ , and for  $B=0$  and  $D=1$  one invariably encounters  $k_m=2\lambda^m$ . The set  $\{k_1, \dots, k_n\}$  will be referred to as a “growth sequence” of length  $n$ . Of course, growth sequences are in general degenerate in the sense that different population landscapes can possess the same growth sequence. The total population after  $n$  generations, denoted by  $\mathcal{N}(n)$ , is then given by

$$\mathcal{N}(n) = \frac{1}{\lambda-1} + \sum_{m=1}^n \frac{\lambda^m - k_m}{\lambda^{2m}}. \quad (4.1)$$

At this point it is useful to note that different growth sequences may accidentally result in the same value for the total population. For example, a single local increase of  $N$  in one generation can be deleted by  $\lambda^2$  local decreases in the next generation. Therefore, an alternative sequence in which nothing changes in those two generations would lead to the same total population.

If we work with the deposition probabilities, related to  $B$  and  $D$  by  $P=B(1-D)$  and  $Q=D(1-B)$ , and define  $S=P+Q$ , the probability for depositing in generation  $m$  any configuration with, say,  $h$  holes,  $f$  flat segments (neither hill

nor hole), and  $\lambda^m - f - h$  hills is given by the following expression which takes into account the number of ways in which the holes and flat segments can be put in the standard combinatorial way,

$$\mathcal{P}_m(h, f) = \binom{\lambda^m}{h} \binom{\lambda^m - h}{f} P^{\lambda^m - f - h} (1 - S)^f Q^h. \quad (4.2)$$

Note that summing this expression over all possible  $h$  and  $f$  gives the total probability,

$$\sum_{h=0}^{\lambda^m} \sum_{f=0}^{\lambda^m - h} \mathcal{P}_m(h, f) = 1, \quad (4.3)$$

which is unity, as it should be.

The probability for having a fixed population increment, that is, a particular value  $k_m = k$ , in generation  $m$ , is given by the following partial sum over the  $\mathcal{P}_m(h, f)$ :

$$\hat{\mathcal{P}}_m(k) = \sum_{h=j(k)}^{[k/2]} \binom{\lambda^m}{h} \binom{\lambda^m - h}{k - 2h} P^{\lambda^m - k + h} (1 - S)^{k - 2h} Q^h. \quad (4.4)$$

Note that  $k$  equals the number of flat segments plus twice the number of holes, so that  $f = k - 2h$ . Here,  $[k/2]$  is equal to  $k/2$  if  $k$  is even, and equal to  $(k - 1)/2$  if  $k$  is odd. Further, the integer  $j(k)$  equals 0 if  $k \leq \lambda^m$ , and  $j(k) = k - \lambda^m$  for  $k > \lambda^m$ . One can verify the normalization

$$\sum_{k=0}^{2\lambda^m} \hat{\mathcal{P}}_m(k) = 1. \quad (4.5)$$

Since the  $k_m$ , for different generations  $m$ , are independent variables, the probability of a given growth sequence is the product

$$\hat{\pi}_n(\mathbf{k}) \equiv \prod_{m=1}^n \hat{\mathcal{P}}_m(k_m), \quad (4.6)$$

where  $\mathbf{k} = (k_1, k_2, \dots, k_n)$ . Consequently, the probability  $\Pi$  of realizing the total population  $\mathcal{N}(n)$  is the sum of the probabilities of all the growth sequences  $\mathbf{k}$  which produce the same value  $\mathcal{N}(n) = \mathcal{N}$ ,

$$\Pi_n(\mathcal{N}) = \sum_{\mathbf{k}}^{(\mathcal{N})} \hat{\pi}_n(\mathbf{k}), \quad (4.7)$$

where the sum takes care of the degeneracy of  $\mathcal{N}$ . In practice this sum contains only a few terms, because typically not many growth sequences lead to the same value for the total population. For large  $n$  the populations  $\mathcal{N}(n)$  converge to the carrying capacities  $K$ , so that the distributions  $\Pi_n(\mathcal{N})$  converge to the *carrying capacity distribution*  $\Pi_\infty(K)$ , or in short  $\Pi(K)$ , which we set out to obtain.

Note that the total probability for the entire process up till any given generation  $n$  is correctly normalized, since

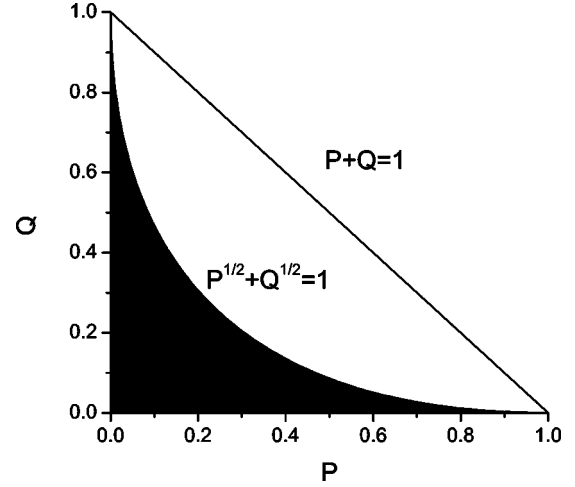


FIG. 2. The dark area in the  $(P, Q)$  plane below the line  $\sqrt{P} + \sqrt{Q} = 1$  corresponds to the “biologically” accessible range of  $P$  and  $Q$ , which can be reached starting from probabilities  $0 \leq B, D \leq 1$  through the relations  $P = B(1 - D)$  and  $Q = D(1 - B)$ . Note that  $P + Q \leq 1$  gives an upper bound on the available “physical” range of  $P$  and  $Q$  in the deposition model.

$$\begin{aligned} 1 &= \prod_{m=1}^n \sum_{k=0}^{2\lambda^m} \hat{\mathcal{P}}_m(k) = \sum_{\mathbf{k}} \prod_{m=1}^n \hat{\mathcal{P}}_m(k_m) = \sum_{\mathbf{k}} \hat{\pi}_n(\mathbf{k}) \\ &= \sum_{\mathcal{N}} \Pi_n(\mathcal{N}). \end{aligned} \quad (4.8)$$

In particular,

$$\sum_K \Pi(K) = 1. \quad (4.9)$$

In closing this section a few technical remarks are in order. Clearly, in the special cases  $P = 0$ ,  $Q = 0$ , or  $P + Q = 1$  the trinomial formulas we have derived, in particular Eqs. (4.2) and (4.4), cannot be used in the present form. Instead, simple binomial expressions should be written down in those cases. Further, in view of the relations  $P = B(1 - D)$  and  $Q = D(1 - B)$  one can verify that the “biological” domain in the  $(P, Q)$  plane occupies only the kite-shaped region below the line  $\sqrt{P} + \sqrt{Q} = 1$ . On this line we have  $B = 1 - D$ . We will discuss later that this is a symmetry line in the  $(B, D)$  plane. Therefore, the present biological application uses only a subset of the parameters of the physical deposition model. This is illustrated in Fig. 2. The relevant kite-shaped region is filled in black. The white area below  $P + Q = 1$  is not accessible in the population model, but it is available in the deposition model.

## V. BACTERIAL POPULATION DISTRIBUTIONS VERSUS ANTIBIOTIC EFFICIENCY

In order to illustrate the carrying capacity distribution and its properties we turn to a few concrete examples. Consider a process with  $B = 0.5$ , representing equally probable nutrient-rich and nutrient-poor patches, and  $D = 0.5$ , corresponding to

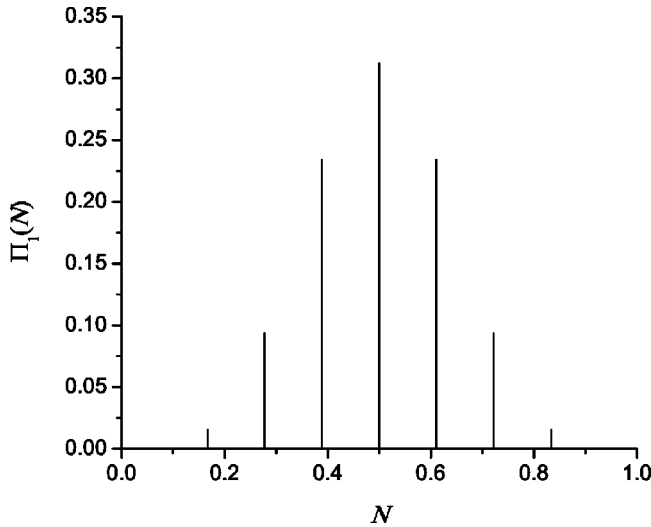


FIG. 3. Population distribution after one generation,  $\Pi_1(\mathcal{N})$ , for  $B=0.5$  and  $D=0.5$ . The most probable population (highest peak) coincides with the initial population.

medium antibiotic strength. It follows that  $P=0.25$  and  $Q=0.25$ . Figure 3 shows the population distribution after one generation,  $\Pi_1(\mathcal{N})$ , for  $\lambda=3$ . Since in the first generation the population is uniquely determined by the growth sequence  $k_1$ , through  $\mathcal{N}(1)=N_0+(\lambda-k_1)/\lambda^2$ , with  $k_1=0, \dots, 2\lambda$ , we have

$$\Pi_1(\mathcal{N}) = \pi_1[k(\mathcal{N})]. \quad (5.1)$$

The probabilities associated with the seven peaks in the figure thus follow directly from Eq. (4.4). Note that the distribution is symmetric about the initial population  $N_0=0.5$ , due to the fact that  $B=D$ .

In the language of fractal geometry [13] Fig. 3 can be called the “generator” of the distribution. If this generator were now applied on a smaller scale to split every peak into seven new peaks, we would obtain a perfect self-similar object, when iterated *ad infinitum*. However, in the second generation the generator is different and has  $2\lambda^2+1$  peaks, 19 in our example. Its width is reduced by a factor of  $\lambda$ , as can be seen from inspection of Eq. (4.1). It is the convolution of the two generators, according to the product expression (4.6) and sum (4.7), which gives the population distribution after two generations. The result is shown in Fig. 4.

In this distribution the seven probability peaks of the first generation are still clearly visible, but they have been split due to the relatively small population shifts obtained in the second generation. The seven structured peaks thus have a width and fine structure determined by the generator of the second generation, and all seven are similar to each other, differing only in their amplitude which is apparent in Fig. 3. Note that the total number of peaks, 73, is significantly smaller than the product  $7 \times 19$ . This is due to overlap of peaks, which results, as discussed previously, from different growth sequences leading to the same population.

As the generations progress, the individual probability peaks can no longer be resolved on the normal population scale. This is the case already after three generations, as Fig.

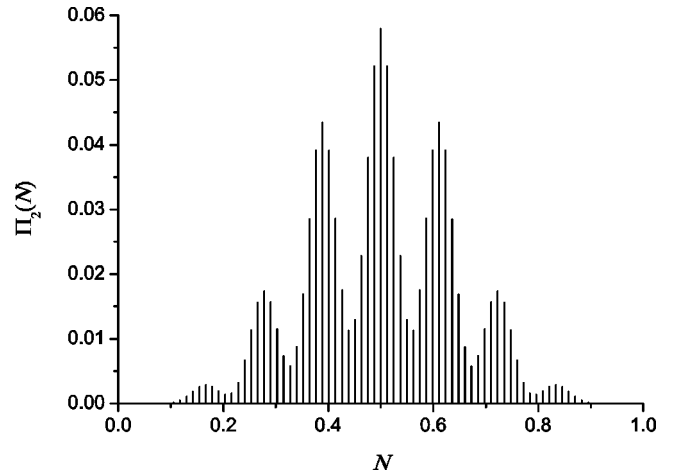


FIG. 4. Population distribution after two generations,  $\Pi_2(\mathcal{N})$ , for  $B=0.5$  and  $D=0.5$ . This distribution arises as the convolution of two generators. The seven peaks originate from the seven populations seen in Fig. 3.

5 shows. There are 703 peaks after three, and 6481 peaks after four generations. The global scaling properties of the distribution can be easily understood if one takes into account that the number of peaks increases by approximately a factor of 9, since the interpeak distance, or minimum population shift, decreases by a factor of  $\lambda^2$  in each generation, as implied by Eq. (4.1). Consequently, in order to preserve the normalization of the total probability the height of the peaks must decrease roughly by a factor of 9 also.

After four generations the population distribution looks nearly identical to that after three generations, provided the height is scaled by roughly a factor of 9. Therefore, Fig. 5 (three generations) already reveals the shape of the population distribution in the limit of a large number of generations, i.e., it gives the carrying capacity distribution  $\Pi(K)$  that we are interested in.

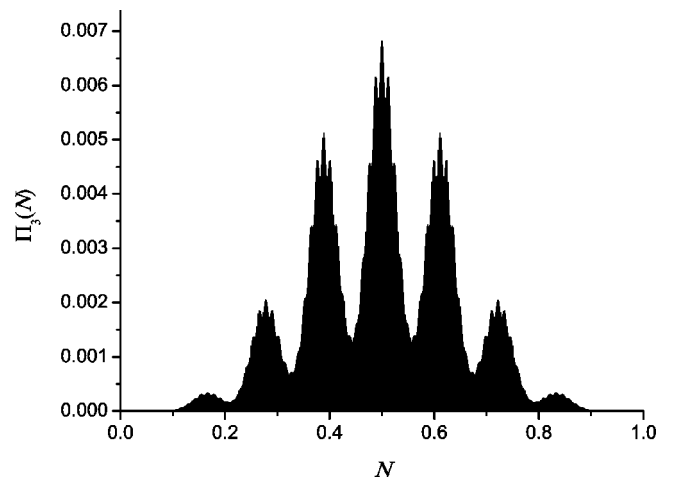


FIG. 5. Population distribution after three generations,  $\Pi_3(\mathcal{N})$ , for  $B=0.5$  and  $D=0.5$ . Notice the self-similarity in the fine structure of the main peaks. The distribution, normalized to unity, gives the probabilities of 703 distinct population values and its shape (but not its height) has almost converged to that of the long-time carrying capacity distribution  $\Pi(K) \equiv \Pi_\infty(\mathcal{N})$ .

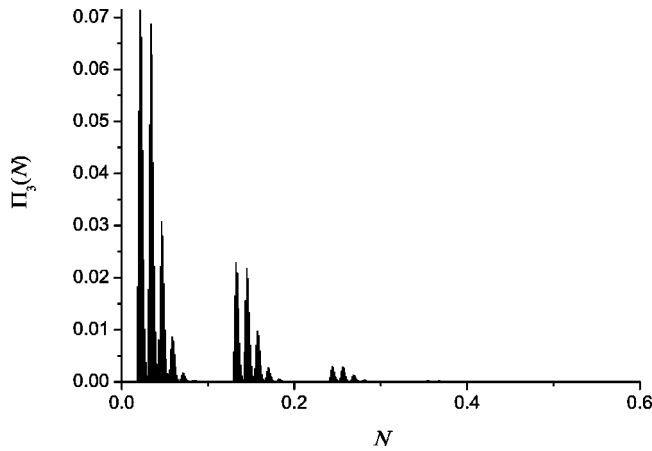


FIG. 6. Population distribution after three generations,  $\Pi_3(\mathcal{N})$ , for  $B=0.05$  (poor nutrient) and  $D=0.95$  (strong antibiotics). The population, initially at  $\mathcal{N}=0.5$ , is strongly suppressed to low values and with small standard deviation. The mean value, 0.067, calculated from Eq. (3.2), is slightly larger than the most probable value.

Besides the analytic calculation, we have carried out simulations of these random processes and obtained population distributions in the form of histograms. Obviously, for a histogram to present accurately a discrete distribution of peaks, the bin width must be smaller than the interpeak separation in population. For example, from these simulations, typically involving  $10^4$  processes for given  $B$  and  $D$ , a histogram with 1000 bins on  $(0,1)$  is obtained which reproduces the analytic results accurately. In view of the fact that little or no changes can be perceived in the shape of the (properly scaled) distribution for generation numbers larger than three, it follows that a histogram with fixed bin size (1000) will converge (without scaling) already after three or four generations and reveal the carrying capacity distribution. In actual experiments a bin size is defined by practical resolution limitations on the counting of bacteria. Therefore, the biologically relevant framework is that which employs a *fixed bin size*.

The example we have chosen in Figs. 3–5 is a typical case in the category of broad carrying capacity distributions with an average value close to (in this case at) the initial homogeneous population  $N_0$ . For medium nutrient levels and medium antibiotic strength the fluctuations are apparently too large for the experimenter to gain “control” over the outcome of the experiment. The situation changes drastically when bacteria in a nutrient-poor environment are exposed to strong antibiotics. In this case a thorough elimination of bacteria results almost certainly. This is shown in Fig. 6.

For birth and death probabilities  $B=0.05$  and  $D=0.95$ , Fig. 6 gives the carrying capacity distribution after three generations. This corresponds to  $P=0.0025$  and  $Q=0.9025$ . Clearly, the population has been suppressed to far below its initial value  $N_0=0.5$ , and the probability is concentrated on the lowest accessible population values, around  $\mathcal{N}\approx 0.06$ . This result is to be expected, and in line with common experience with the effect of antibiotics on bacteria in a nutrient-poor medium.

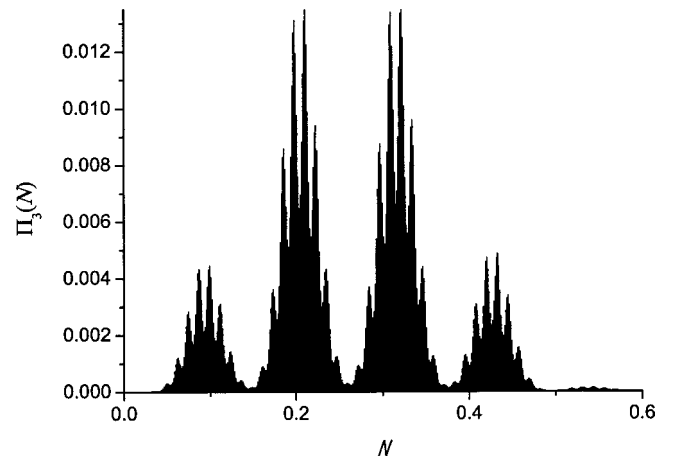


FIG. 7. Population distribution after three generations,  $\Pi_3(\mathcal{N})$ , for  $B=0.5$  and  $D=0.99$ . In spite of the strong antibiotics the nutrient-rich surface allows the population to survive at, on average, half the initial value, and with large fluctuations. Notice that the mean value, 0.264, calculated from Eq. (3.2), is roughly in between the two most probable values.

Possibly a more surprising result from this model is what happens when medium nutrient level is combined with strong (or very strong) antibiotics. If we take  $B=0.5$  and  $D=0.99$ , leading to  $P=0.005$  and  $Q=0.495$ , we obtain the carrying capacity distribution shown in Fig. 7. The following properties are conspicuous: (i) the population is entirely shifted to well below its initial value  $N_0=0.5$ , (ii) the distribution is broad, and (iii) the average population is about half the initial population. It appears that the antibiotic has failed in two respects. The population has not been suppressed completely, and it is difficult to predict the eventual asymptotic population due to the large fluctuations. Mathematically, this insufficiency can be traced to be caused, not by the medium abundance of nutrient-rich patches in itself, since only very little growth is observed ( $P=0.005$  is very small), but by a substantial reduction of the antibiotic efficiency. This reduction, from  $D=0.99$  in biological parameter space, to  $Q=0.495$  in physical parameter space, is due to the *indirect* effect of nutrient-rich spots on antibiotic strength through  $Q=D(1-B)$ . Indeed, on 50% of the biofilm the antibiotic efficiency is spent on taking out only the newly produced bacteria, since  $B=0.5$ , and only on the remaining 50% of the area the initially existing population gets (almost) killed eventually, so that we can understand that  $\bar{N}(n) \rightarrow 0.255$ , for  $n \rightarrow \infty$ .

The few representative cases we have discussed up to now are the most interesting ones which can be studied within this very simple model. We do not need to devote special attention to the limits  $B \approx D \approx 0$  or, equivalently,  $B \approx D \approx 1$ , for which the distribution remains sharply concentrated around the initial value, so that the outcome of experiments is simple to predict. In the following section we elaborate on the behavior of the most probable carrying capacity and its probability as a function of the birth and death rates, i.e., of  $B$  and  $D$ .

**VI. MOST PROBABLE CARRYING CAPACITY AND ITS PROBABILITY**

With regard to an actual experiment it is important to predict the *most probable* carrying capacity,  $K^*$ , that will be observed, and its probability of occurrence,  $\Pi(K^*)$ , given the birth and death probabilities  $B$  and  $D$ . In general  $K^*$  differs from the mean  $\bar{K}$ . We have studied these properties of the model for rescaling factors  $\lambda=2$  and  $\lambda=3$ . Differences in rescaling factor are seen to lead to quantitative differences only, not essential for our discussion. Here we report on the results for  $\lambda=3$ .

Since the population distributions converge rapidly with increasing generation number, the results for the first generation (the “generator”) determine to a very good approximation the relative importance of the peaks in the final distributions, as well as the population values associated with the peaks. Therefore, we can restrict our attention to the *first generation* when studying the most probable carrying capacity and its probability *qualitatively*, and work with the most probable population  $\mathcal{N}^*$  and its probability  $\Pi_1(\mathcal{N}^*)$ . In the Appendix we give the analytic expressions for the probabilities of the populations after one generation.

There are two lines of symmetry in the model, which merit separate attention. The line  $B=D$  is a symmetry line in the sense that the population distributions for  $B>D$  are the mirror images, reflected about  $N=0.5$ , of the distributions with  $B$  and  $D$  interchanged. On the line  $B=D$  the average population remains equal to the initial population. There is no net growth (see Sec. III). One would therefore suspect that, when the antibiotic strength precisely compensates the nutrient abundance, the most probable population after the experiment equals the initial population. This is indeed the case. However, unless  $B$  is sufficiently close to 0 or to 1, the fluctuations are large and the probability  $\Pi_1(0.5)$  of observing the most probable population is less than 50%. This is illustrated in Fig. 8 (case  $B=D$ ).

The second symmetry concerns the substitution of  $B$  by  $1-D$ , and of  $D$  by  $1-B$ . Clearly, this operation leaves  $P$  and  $Q$  unchanged, and therefore the results are invariant. The line  $B+D=1$  thus acts like a mirror in the  $(B,D)$  plane. The probability  $\Pi_1(\mathcal{N}^*)$  along this line shows interesting cornerlike singularities where the most probable population makes a jump. In a statistical mechanical context what we are doing is similar to minimizing the “free energy”  $F=-\Pi_1(\mathcal{N})$  with respect to  $\mathcal{N}$ , for every  $B$ , and obtaining the minimum-free-energy (maximum- $\Pi_1$ ) curve which displays corners at points where two “phases” (values of  $\mathcal{N}^*$ ) coexist. Here, the relevant  $\mathcal{N}$  are restricted to the seven population values generated in the first generation (Fig. 3), so that the curve can have (at most) six corners. Figure 8 shows the probability of the most probable population along this line (case  $B+D=1$ ). Although this curve has been calculated only for the first generation, it is important to keep in mind that it is already a good approximation to the probability of the most probable carrying capacity  $K^*$ , defined in the limit of a large number of generations. That curve  $\Pi(K^*)$  must also display cornerlike singularities, representing jumps in  $K^*$ , at values of  $B$  (or  $D$ ) close to the singularities exhibited in Fig. 8.

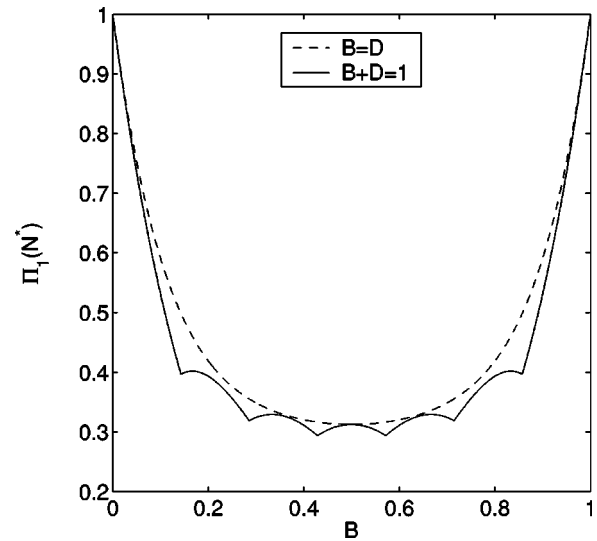


FIG. 8. Probability of the most probable population after one generation, as a function of  $B$ , for the special symmetry lines  $B=D$  (dashed line without singularities; along this line  $\mathcal{N}^*=\bar{N}=N_0=0.5$ ) and  $B+D=1$  (solid line with six corner singularities).

These jumps in  $K^*$  occur when two main peaks in the distribution (see Fig. 7 for example) exchange maximum height.

A global plot of the most probable population  $\mathcal{N}^*$  after one generation, in the domain  $0 \leq B, D \leq 1$  is presented in Fig. 9. The two symmetries we discussed can be seen in this plot. The singularities, in the form of terrace border lines, represent the “coexistence” of two distinct values of  $K^*$ . These lines run roughly parallel to lines of constant  $B-D$ , so that, to a crude first approximation, the most probable population depends mainly on the difference  $B-D$ . Recall that the average population  $\bar{N}$  depends *only* on  $B-D$ , according to Eq. (3.1).

The probability  $\Pi_1(\mathcal{N}^*)$  as a function of  $B$  and  $D$  is shown in Fig. 10. It displays lines of cornerlike singularities

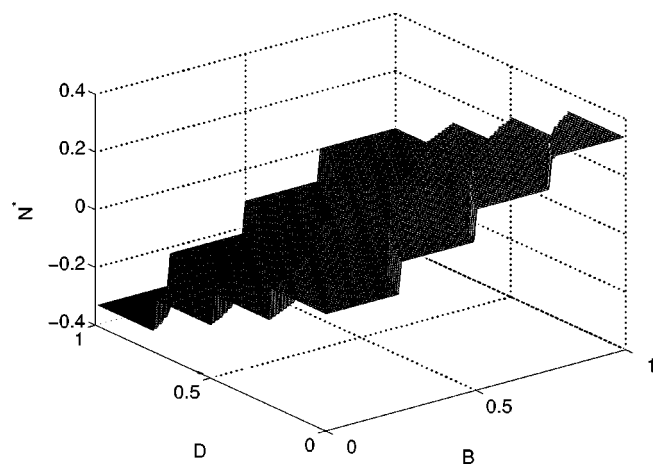


FIG. 9. Most probable population after one generation as a function of  $B$  and  $D$ . The staircase structure reveals where two values of  $\mathcal{N}^*$  exchange maximum probability. The model symmetries are apparent and help interpret Fig. 8 and Fig. 10.

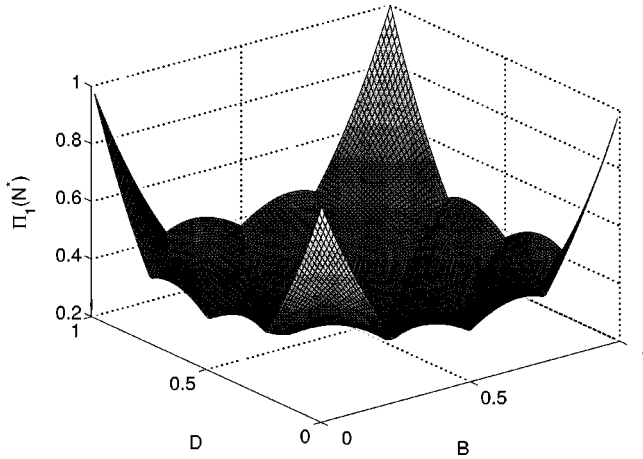


FIG. 10. Probability of the most probable population after one generation, as a function of  $B$  and  $D$ . Two special lines along this surface are shown in Fig. 8. Notice that the border lines at  $B=0$  or  $B=1$  display three corner singularities, as do the lines for  $D=0$  or  $D=1$ .

precisely where the terrace borders occur in Fig. 9. Note that a sharp population distribution is only found near the four points where  $B$  and  $D$  are close to 0 or 1.

In order to quantify this further we have calculated the standard deviation  $\Sigma_1$  of the distribution after one generation, as a function of  $B$  and  $D$ . This quantity is defined through

$$(\Sigma_1)^2 = \frac{1}{2\lambda + 1} \sum_{k=0}^{2\lambda} [\mathcal{N}_k - \bar{N}(1)]^2 \hat{P}_1(k), \quad (6.1)$$

with  $\mathcal{N}_k \equiv 1/(\lambda - 1) + (\lambda - k)/\lambda^2$  and, from Eq. (3.2),  $\bar{N}(1) = 1/(\lambda - 1) + (B - D)/\lambda$ . Explicit expressions for the  $\hat{P}_1$  are given in the Appendix. The standard deviation is shown in Fig. 11. Like the average population, the standard deviation is a smooth function of  $B$  and  $D$ , and illustrates clearly that a broad population distribution is generic.

## VII. CONCLUSIONS AND A POSSIBLE EXPERIMENTAL TEST

Keeping in mind possible relevance of this hierarchical model to towering pillar biofilms, as discussed in Sec. II, we recapitulate here the main model ingredients. The model contains three parameters: birth probability  $B$ , death probability  $D$ , and rescaling factor  $\lambda$ .  $B$  essentially reflects the fraction (or quality) of nutrient-rich area on the surface, and  $D$  the density (or quality) of bactericidal agents. The rescaling factor  $\lambda$  sets the characteristic bare decay rate (Sec. III) and controls the fragmentation—in space—of the nutrient-rich patches and the antimicrobial activity, mimicking diffusion and transport. The main role of  $\lambda$  has been to generate the exponentially rapid saturation of the population by decreasing—uniformly in space—the amount of offsprings in each generation and simultaneously increasing uniformly antimicrobial resistance. This mimics, for example, a nutrient or temperature drop and biofilm development, respectively,

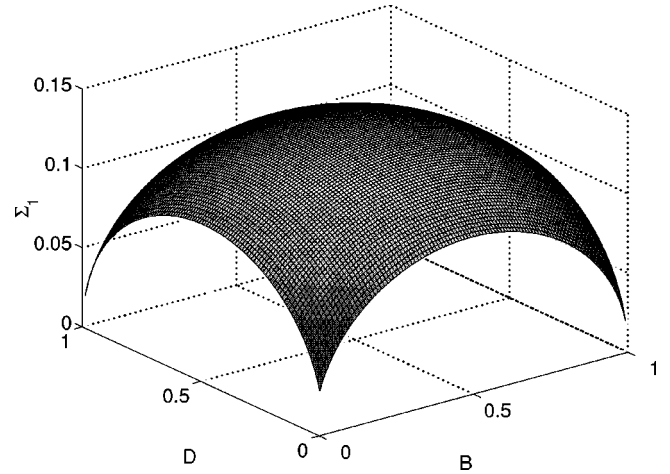


FIG. 11. Standard deviation  $\Sigma_1$  of the population distribution after one generation, vs  $B$  and  $D$ . We have defined  $\Sigma_1 \equiv \sqrt{2\lambda + 1} \hat{\Sigma}_1$ . Notice that only extreme values of  $B$  and  $D$  (near the corners of the square, where  $\Sigma_1$  approaches zero) lead to a sharp distribution and easily predictable populations of individual samples.

as discussed in Sec. II. Through the action of  $\lambda$  the model becomes hierarchical and this leads to a finite carrying capacity (“freezing” or stagnation). Undoubtedly, the use of just one parameter  $\lambda$  for inducing all these dynamical effects, in the interest of simplicity and transparency of the model, cannot be more than a first crude step towards a more realistic and refined approach.

The growth of the population thus acquires a hierarchical structure, apparent in the fractal population “landscapes” (Fig. 1), and expressed by a (nearly) self-similar carrying capacity distribution (Figs. 3–7), the mathematics of which has been discussed using elementary notions of fractal geometry. The main conclusion from studying these distributions is that for generic values of  $B$  and  $D$  a broad range of carrying capacities can be observed, and the outcome depends largely on the sample used. Ensemble averaging is necessary for predicting statistically relevant properties of this type of growth.

The question now arises whether this model is relevant to an experiment in which bacteria capable of forming a biofilm on an inhomogeneous nutrient field are exposed to antibiotic or protein spray and subsequently put in a refrigerator or an oven (for about a day, with  $\Delta T \approx 1$  °C/h). The applicability of the model relies primarily on the determination of the model parameters starting from experimental system parameters. In our discussion we have taken  $\lambda=3$ , having in mind that the linear size of a nutrient-rich patch or an antibiotic drop is roughly one third of the inoculation line. This length ratio can be determined easily in practice and the rescaling factor can be adjusted, or, of course, two separate rescaling factors can be introduced if necessary. The external cooling (or heating) rate, taking the bacteria away from optimal growth conditions, is assumed to be adjusted so that the processes come to a halt in about four to five generations. The quality of the nutrient and the strength of the antibiotic, in-

corporated in  $B$  and  $D$ , can be tuned experimentally by dilution, for example. Alternatively, one can work with a fixed amount of nutrient, all of which is placed initially on the substrate in a nonuniform way. In this case, without “refueling,” the population will come to a halt with no need to change the temperature of the sample.

State-of-the-art experiments allow a simultaneous counting of many samples (say,  $10^4$ ) on a microarray in order to obtain carrying capacity distributions, much like is done in ensemble averaging. In sum, a direct experimental check of this model is feasible, and would be worthwhile, before introducing theoretical refinements which undoubtedly are necessary to make the model more realistic, but on the other hand compromise the insight that can be gained using only very few key parameters.

#### ACKNOWLEDGMENTS

We thank Ralf Blossey for suggesting the possible applicability of the hierarchical population model to biofilms. We are grateful to Reiner Kree, Joachim Krug, Valeria del Prete, Güler Ergün, Inma Rodriguez Ponce, and Claudiu Giuraniuc for constructive comments on the model. This research was supported by the Flemish Program FWO-G.0222.02 “Physical and Interdisciplinary Applications of Novel Fractal Structures.” K. S.-W. was supported by the Foundation for Polish Science.

#### APPENDIX: PROBABILITIES OF THE POPULATION AFTER ONE GENERATION (CASE $\lambda=3$ )

In this appendix we give the analytic expressions used in the calculations of the most probable population and its probability after one generation (Sec. VI). The rescaling factor is  $\lambda=3$ . In terms of the auxiliary probabilities

$$P=B(1-D) \quad \text{and} \quad Q=D(1-B), \quad (\text{A1})$$

with  $0 \leq B, D \leq 1$ ; and in terms of  $S=P+Q$ , we obtain, using Eq. (4.4),

$$\hat{P}_1(0)=P^3,$$

$$\hat{P}_1(1)=3P^2(1-S),$$

$$\hat{P}_1(2)=3P(1-S)^2+3P^2Q,$$

$$\hat{P}_1(3)=(1-S)^3+6P(1-S)Q,$$

$$\hat{P}_1(4)=3(1-S)^2Q+3PQ^2,$$

$$\hat{P}_1(5)=3(1-S)Q^2,$$

$$\hat{P}_1(6)=Q^3. \quad (\text{A2})$$

- 
- [1] M. Eden, in *Proceedings of the 4th Berkeley Symposium on Mathematical Statistics and Probability*, edited by F. Neyman (University of California Press, Berkeley, 1961), Vol. 4, p. 223.
- [2] T. Vicsek, M. Cserző, and V.K. Horváth, *Physica A* **167**, 315 (1990).
- [3] H. Fujikawa and M. Matsushita, *J. Phys. Soc. Jpn.* **58**, 3875 (1989); M. Matsushita and H. Fujikawa, *Physica A* **168**, 498 (1990).
- [4] T.A. Witten and L.M. Sander, *Phys. Rev. Lett.* **47**, 1400 (1981).
- [5] E. Ben-Jacob, I. Cohen, O. Shochet, A. Tenenbaum, A. Czirók, and T. Vicsek, *Phys. Rev. Lett.* **75**, 2899 (1995); E. Ben-Jacob, O. Shochet, A. Tenenbaum, I. Cohen, A. Czirók, and T. Vicsek, *Nature (London)* **368**, 46 (1994).
- [6] T. Neicu, A. Pradhan, D.A. Larochelle, and A. Kudrolli, *Phys. Rev. E* **62**, 1059 (2000).
- [7] K.A. Dahmen, D.R. Nelson, and N.M. Schnerb, e-print cond-mat/9807394.
- [8] P.K. Singh, M.R. Parsek, E.P. Greenberg, and M.J. Welsh, *Nature (London)* **417**, 552 (2002); see also H. Pearson (unpublished).
- [9] J. D. Murray, *Mathematical Biology*, Biomathematics Vol. 19 (Springer-Verlag, Berlin, 1993).
- [10] J.O. Indekeu and G. Fleerackers, *Physica A* **261**, 294 (1998).
- [11] J.O. Indekeu, G. Fleerackers, A.I. Posazhennikova, and E. Bervoets, *Physica A* **285**, 135 (2000).
- [12] See, for example, S. W. Hermanowicz’ homepage on the Internet. On the website [www.ce.berkeley.edu/~hermanowicz/](http://www.ce.berkeley.edu/~hermanowicz/) one can find relevant biofilm images, obtained by U. Schindler (Munich). For a forthcoming overview, see S. W. Hermanowicz, in *Biofilm Structure: an Interplay of Models and Experiments*, edited by S. Wuerz, P. A. Wilderer, and P. L. Bishop (International Water Association Publishing, Colchester, 2003).
- [13] B. Mandelbrot, *The Fractal Geometry of Nature* (Freeman, New York, 1983).
- [14] S.W. Hermanowicz, U. Schindler, and P. Wilderer, *Water Sci. Technol.* **32**, 99 (1995).
- [15] S.W. Hermanowicz, *Water Sci. Technol.* **39**, 107 (1999); *Math. Biosci.* **169**, 1 (2001).